Solid State Lithionics based Gas-Sensing and Memristive Device

M.Sc. Thesis

By

Manavi Rajan

DEPARTMENT OF CHEMISTRY

INDIAN INSTITUTE OF TECHNOLOGY INDORE

Solid State Lithionics based Gas-Sensing and Memristive Device

A THESIS

Submitted in partial fulfilment of the

Requirements for the award of the degree

of

Master of Science

by

Manavi Rajan

DEPARTMENT OF CHEMISTRY

INDIAN INSTITUTE OF TECHNOLOGY INDORE

MAY 2024

INDIAN INSTITUTE OF TECHNOLOGY, INDORE

CANDIDATE'S DECLARATION

I hereby certify that the work which is being presented in the thesis entitled "**Solid State Lithionics based Gas Sensing and Memristive Device"** in the partial fulfilment of the requirements for the award of the degree of **MASTER OF SCIENCE** and submitted in the **DEPARTMENT OF CHEMISTRY, Indian Institute of Technology Indore**, is an authentic record of my own work carried out during the time from July 2023 to May 2024 under the supervision of Dr. Pravarthana Dhanapal, Assistant Professor, Department of Chemistry, IIT Indore. The matter presented in this thesis has not been submitted by me for the award of any other degree of this or any other institute.

06-05-24
Signature of the student with date
(Manavi Rajan)

This is to certify that the above statement made by the candidate is correct to the best of my/our knowledge.

06-05-24

Signature of Thesis Supervisor with date
(Dr. Pravarthana Dhanapal)

Manavi Rajan has successfully given her M.Sc. Oral Examination held on 8th May 2024

Signature of Supervisor M.Sc. thesis

Date: 06-05-24

Convenor, DPGC

Date:

Signature of PSPC member 1
Date:

Signature of PSPC member 2
Date:

ACKNOWLEDGMENTS

It's an excellent opportunity to thank everyone who has helped me in various ways during the year. I'd like to begin by expressing my heartfelt appreciation to my supervisor **Dr. Pravarthana Dhanapal** and my PSPC committee members **Dr. Selvakumar Sermadurai** and **Prof. Anjan Chakraborty** for their valuable guidance.

I would like to express my sincere appreciation to my research supervisor **Dr. Pravarthana Dhanapal** for his guidance, constant encouragement and suggestions throughout my M.Sc. project. I was very fortunate to be under his kind guidance, which has made me gain valuable knowledge in the subject. His confidence, enthusiasm, and dedication have been always inspirational. His deep insights and suggestions helped me a lot. I also take this opportunity to thank our honourable Director **Prof. Suhas Joshi** and Head of the Chemistry Department, **Prof. Tushar Kanti Mukherjee,** IIT Indore for providing the infrastructure and necessary environment to carry out research. I would also like to thank the entire faculty of IIT Indore and SIC for consistently showing a supporting gesture.

I would like to thank **Prof. Suman Mukhopadhyay** for his support throughout the year, **Prof. I.A. Palani**, Department of Mechanical Engineering for RF Sputtering facility and **Dr. Vinod Kumar**, Department of Metallurgical Engineering and Material Science for their lab facilities.

I thank **Mr. Mayur Dhake and Mr. Pranjal Shrimali and Mr. Gokul Pillai,** Department of Metallurgy and Material Science for their technical support and assistance throughout the year. I would like to thank **Ms. Nisha Kumari** for helping me with this project.

Most importantly, it would have been impossible for me to reach here without the support of my family members.

I would like to express my gratitude to my parents, seniors and friends for their constant motivation throughout my life, for cheering me up

during the tough times of this journey and for always being understanding and supportive.

Manavi Rajan
Department of Chemistry
IIT INDORE

Dedicated to

My Family

ABSTRACT

Gas sensing devices play a major role in many industries. From the sensing of toxic gases from industrial waste, breath analysis to diagnose diseases and gas sensing in agriculture industry, its importance is multifold. Specifically in the agricultural industries, the use of sensors to monitor fruit ripening is necessary to minimize the associated losses. The focus of this thesis is to not only develop an ethylene gas sensor but also see the effects of doping towards its properties. We have employed solid state ionics to modulate the Li-ion concentration by in-situ doping into ZnO. The utility of the sensor has been tested with ethylene gas as well as with real fruits to demonstrate the success of this device.

TABLE OF CONTENTS

LIST OF FIGURES

ACRONYMS

Ppm : parts per million

SR : Sensor Response

Temp : Temperature

eV : electron volts

XRD : X Ray Diffraction

SEM : Scanning Electron Microscopy

AFM : Atomic Force Microscopy

Chapter 1: Introduction

1.1 Solid State Ionics

Combining knowledge from different disciplines often leads to the generation of innovative ideas and novel solutions to existing research challenges. Multidisciplinary research facilitates the cross-pollination of ideas of scientists from different backgrounds to develop hybrid concepts and methodologies. Solid-state ionics is a vibrant and multi-disciplinary research field that combines physics, chemistry and material science and explores the behavior, properties, and applications of ions in solid materials. Solid-state ionics play a pivotal role in developing next-generation energy storage devices, particularly solid-state batteries. The name “Solid State Ionics” was first used by Takahashi at the 1972 fall meeting of the American Electrochemical Society[1]. It is an interdisciplinary field that leverages the electrochemical phenomena due to ionic motion to develop devices for specific applications. Initially, it focused only on the solid electrolytes required for batteries but has now become more all-encompassing; including gas sensors, actuators, memory resistors, electrochemical switches etc.

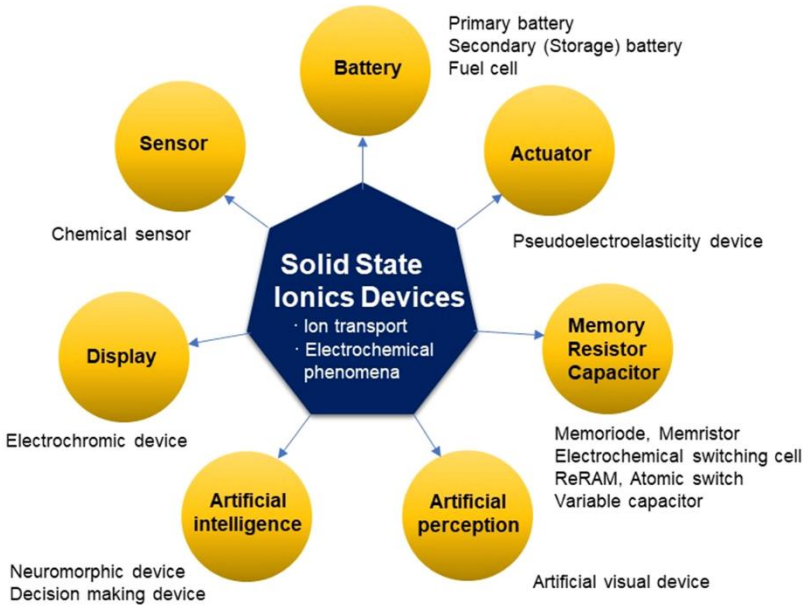

Figure 1: Various solid state ionics devices operated by utilizing ion transport and electrochemical phenomena in solids [1].

The simultaneous advancements in the semiconductor industry, material science and thin film technologies have made possible the transition from bulky, power-hungry devices to cost-efficient and low power consuming solid state devices. These cater to various functional applications such as gas sensing, catalysis, artificial intelligence etc. [NO_PRINTED_FORM] 2

In the 1960s and 70s, the groundwork for Li-ions was being laid that garnered more attention when the first Li-ion battery was made by John B. Goodenough in 1980 at the University of Oxford[3] . This marked the beginning of a revolution in portable electronics. There were multiple reasons for choosing lithium-ion in batteries. It is the 3rd lightest element in the periodic table, and has a small ionic radius thus a high diffusion coefficient. Further research on the interaction of Li ions with various materials used in the electrodes were investigated over the years to understand the mechanism of charge storage. Alloying, conversion and insertion are the 3 main types into which this interaction has been classified[4]. These insights into the reaction of lithium with other elements has allowed exploiting the versatility of this element for applications other than batteries.

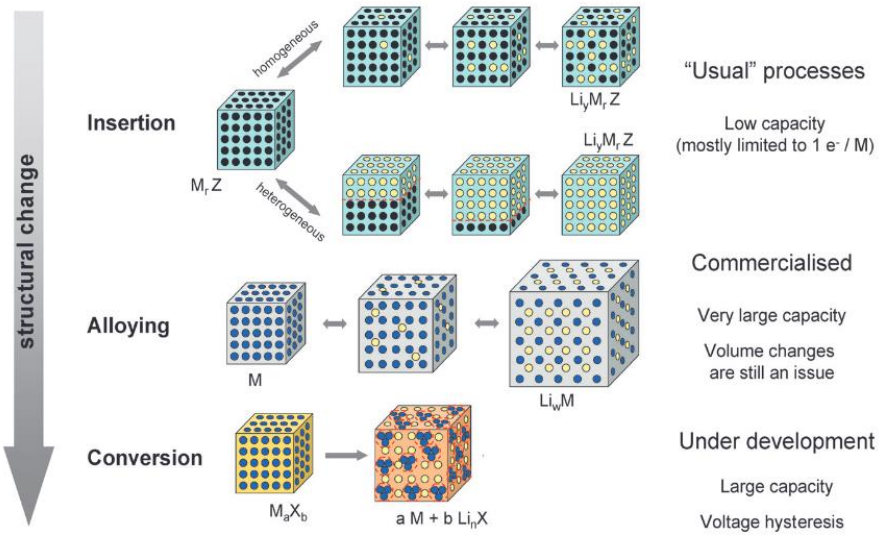

Figure 2: A schematic representation of the different reaction mechanisms observed in electrode materials for lithium batteries. Black circles: voids in the crystal structure, blue circles: metal, yellow circles: lithium[5]

This project throws light on the gas sensing and memristive applications of solid state ionics-based devices owing to the following advantages.

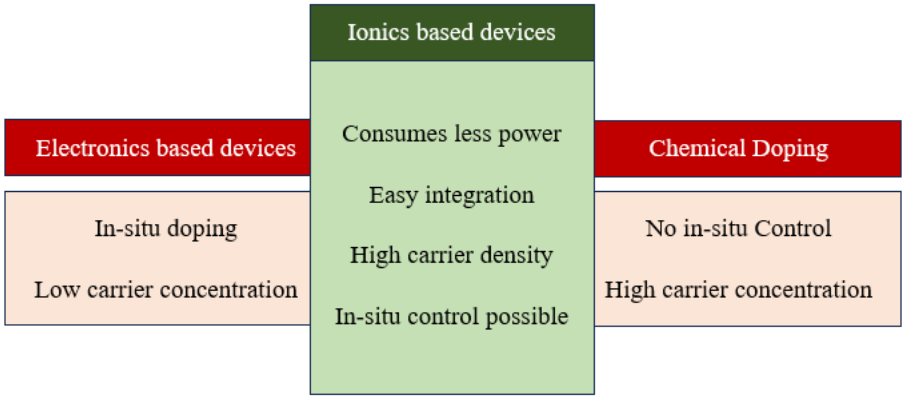

Figure 3 : A comparison between electronic, ionic and chemical doping

1.2 Ethylene Sensing

The focus of this project is on 2 main devices namely gas sensor and memristor. The gas sensing device is aimed at sensing ethylene gas. Ethylene is the plant-ripening hormone. Ethylene production in fruits increases with time on ripening. As a result, it diffuses out of the skin

into the atmosphere. Timely monitoring of ethylene gas can help prevent wastage of agricultural produce. The agricultural sector significantly contributes to the GDP, making up approximately 5,688 billion rupees, or nearly 21% of the total. This sector serves as the primary source of income for 55% of the population. Despite its profitability, there are associated losses that can be reduced through the appropriate use of technology. When agricultural products start to deteriorate, they release specific gases that may go unnoticed by humans. Gas sensors can play a crucial role in detecting these gases, preventing the wastage of agricultural produce, and ultimately reducing landfill accumulation. Furthermore, ensuring food safety standards is a challenge, especially when catering to a large population. To address this issue, it becomes essential to develop rapid, efficient, and reliable gas-sensing devices. Although electrochemical gas sensors with liquid electrolytes have limitations such as low cyclability and selectivity, replacing them with solid-state electrolytes has shown improved performance [6]. The type of gas causing chemical changes may vary depending on whether it is a processed food item or fresh agricultural produce. This study focuses on detecting ethylene gas, which is emitted during the ripening of fruits. Based on the ripening process, fruits are classified as climacteric or non-climacteric. In the case of climacteric fruits, a very well-established biochemical pathway known as Yang's cycle[7] (Fig.1) explains the production of ethylene in the ripening stages. The gas-sensing device operates on the principle that the reversible adsorption of gas alters its electrical properties, indicating the device's sensitivity. Based on the type of gas, there is an increase or decrease in the resistance of the thin film. Reducing gases decreases the width of the depletion layer on adsorption, which results in a decrease in resistance and vice-versa for oxidizing gases[8] . While traditional gas sensors use sensing and reference electrodes made of platinum (Pt) metal, this research explores the possibility of substituting the sensing electrode with anode materials capable of forming alloys or undergoing conversion reactions with lithium ions. This substitution aims to enhance selectivity and eliminate the need for high operating temperatures.

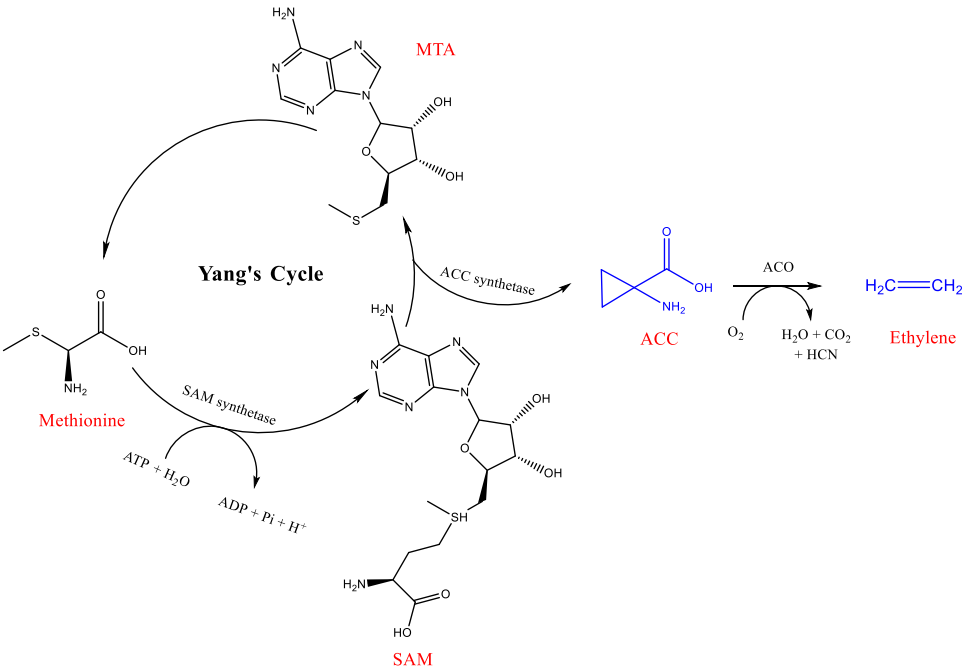

Figure 4: Yang's cycle

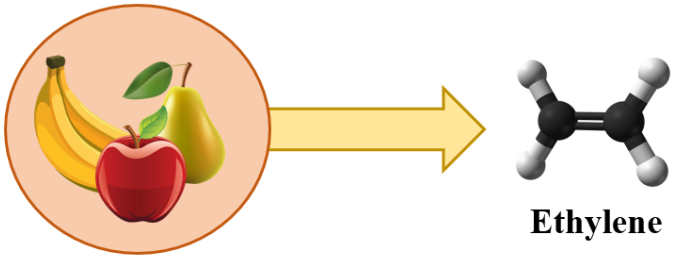

Figure 5: Fruit ripening is caused by the ripening hormone ethylene

1.3 Challenges in ethylene sensing

Ethylene, C_2H_4, is a basic hydrocarbon molecule with significant roles in nature. Its minimal functional features complicate the task of detecting it with high sensitivity. Its low reactivity and small molecular size further add to the difficulty. Therefore, developing highly sensitive sensors to detect ethylene poses a substantial challenge. Various methods have been used to detect ethylene[9]. Our focus is to develop a cost-effective ethylene gas sensor with tuneable properties.

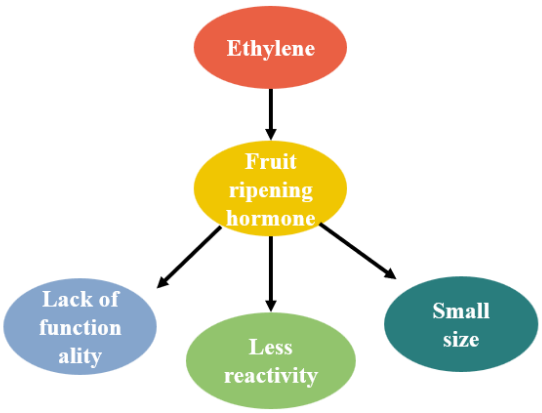

Figure 6: Challenges in ethylene sensing

1.4 Focus of this work

1.4.1 The Sensing Electrode

The structure of a gas sensor consists of the top electrode which is the sensing electrode and a bottom electrode. The choice of material is very crucial for the top electrode. We have chosen ZnO as the sensing electrode in this work. ZnO has been widely studied for its use in gas sensing. This can be attributed to the fact that it is a wide bandgap semiconductor (band gap of ~3.37 eV at room temperature) so its properties can easily be tuned[10] . A detailed list of gas sensors based on ZnO has been discussed in Chapter 2.

ZnO has a high surface-to-volume ratio, especially when synthesized in nanostructures such as nanoparticles, nanowires, or nanorods. This high surface reactivity makes it very effective in adsorption of gases, leading to significant changes in its electrical properties when exposed to different gases. ZnO is chemically stable and mechanically robust, which makes it suitable for use in harsh environments[11]. Its stability ensures that the sensor characteristics do not degrade significantly over time, which is important for long-term applications. ZnO can be synthesized using a variety of methods, including chemical vapor deposition[11,12], sol-gel techniques[13], and thermal decomposition. These methods can be adjusted to control the morphology and size of ZnO

particles, which are crucial parameters for optimizing their sensing properties. Compared to other semiconducting materials, ZnO is relatively inexpensive and abundant, making it a cost-effective choice for sensor development. This is particularly important when scaling up the technology for commercial applications. ZnO is a non-toxic material, making it an environmentally friendly choice for sensor applications. This aspect is increasingly important as environmental regulations become more stringent. The properties of ZnO can be modified by doping with other elements (like Al, Ga, etc.), which can improve its gas sensing performance, such as sensitivity, selectivity, and operational temperature range. This adaptability allows for the tailoring of sensors for specific applications. These attributes make ZnO a highly attractive option for both research and practical applications in gas sensing, leading to its extensive utilization in academia and industry.

1.4.2 The substrate

Conventionally, ZnO films are deposited onto substrates that are insulating in nature. Here, we have chosen Li-Ion Conducting Glass Ceramic as the substrate (LICGC). This acts as a solid electrolyte and can thus be used as a source of Li-ions for facilitating the lithiation of ZnO. It has a low surface roughness assuring intimate contact with the film being deposited. The electrochemical studies were performed for the substrate as well as the combined device and have been discussed in Chapter 4.

1.5 Methodology

Thin films were used to fabricate the device. The development of better devices is dependent on the technology available for their fabrication. Thin film technology plays a significant role in the field of solid-state ionics as it makes possible the miniaturization of existing devices and enhances the cost-effectiveness. This technology involves depositing thin layers of materials onto a substrate to create functional structures. In the context of solid-state devices, such as integrated circuits (ICs), transistors, and sensors, thin film technology offers

several advantages.

1.5.1 Thin film fabrication methods

Thin film fabrication methods are diverse and varied. Some are affordable on the lab scale but aren't feasible on an industrial scale. Some of the most common thin film fabrication methods are:

(a) Pulsed Laser Deposition (PLD):
(b) RF Sputtering
(c) Spin coating
(d) Atomic Layer deposition
(e) Molecular beam epitaxy
(f) Chemical vapour deposition
(g) Doctor blading

Our focus is mainly on RF sputtering, spin coating and doctor blading as they are scalable methods.

A. Pulsed Laser deposition

Pulsed Laser Deposition (PLD) is a thin film deposition technique that utilizes a laser to ablate material from a target and deposit it onto a substrate. This method allows for the precise control of film thickness and composition, making it suitable for the fabrication of complex materials with diverse applications.

B. RF Sputtering

Radiofrequency (RF) sputtering is a thin film deposition technique used to create thin layers of material on a substrate. The target material is bombarded with ions in a radiofrequency-generated plasma, leading to the ejection of atoms or molecules from the target. These ejected particles then deposit onto a substrate, forming a thin film. RF sputtering is widely employed in various industries for applications.

C. Spin coating

The working principle of spin coating involves the controlled

application of a liquid solution or suspension onto a spinning substrate. As the substrate spins, centrifugal force acts on the liquid, causing it to spread evenly across the substrate surface. The rapid rotation results in a thin and uniform layer of the liquid being deposited on the substrate.

D. Doctor blading

It is one of the most widely employed fabrication methods industrially owing to its simple procedure. A slurry mixture is made and cast onto one side of the substrate and then spread by a blade to obtain uniformity.

1.6 Organization of the Thesis

Chapter 1: This chapter thoroughly explains solid state ionics and gas sensing along with a brief outline of the focus of this project. It also explains the challenges with ethylene sensing.

Chapter 2: This chapter includes the motivation behind the work and review of past work done in the same field.

Chapter 3: This chapter includes details of the chemicals as well as the method employed to fabricate the device. It describes the procedure followed for doctor blading and RF sputtering along with their respective schematics.

Chapter 4: This chapter includes all the obtained results.

Chapter 5: This chapter concludes the work done in this thesis, along with the scope for future applications.

Chapter 2: Literature Review

A sensor is a device that transforms a physical quantity into a signal that can be interpreted by a person or an electronic device. It is often referred to as a detector or a transducer. A gas sensor is a type of transducer that identifies gas molecules and generates an electrical signal whose intensity correlates with the gas concentration. The detection of gases primarily involves chemical processes, whereas the conversion of this detection into a signal involves physical processes. This implies that the detection is highly influenced by external conditions, particularly temperature. The sensitivity of the sensor response depends greatly on both the type of receptor employed and the temperature at which it operates.

There are many types of gas sensors based on working principles and structure. Out of these, the chemiresistive gas sensors widely employ metal oxide semiconductors for the sensing layer. Chemiresistive gas sensors function based on the principle of changes in electrical resistance that occur when the semiconductor material interacts with gases. By monitoring these resistance changes when exposed to various gases, one can measure the resistance with straightforward instrumentation. The adsorption of the target gas onto the semiconductor surface and its subsequent reaction with oxygen species already present on the surface leads to a variation in the semiconductor's electrical resistance, which corresponds to the concentration of the gas.

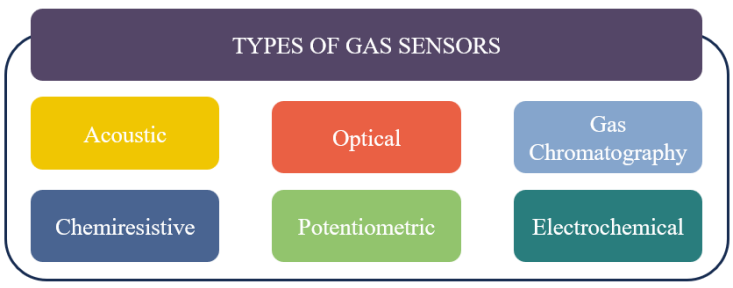

Figure 7: Types of gas sensors

Semiconductor oxides like TiO_2, ZnO, SnO_2, and NiO demonstrate promising capabilities as sensing materials for a broad range of gases, owing to their remarkable properties and stability. However, only a few of these oxides are suitable for actual sensor technology applications unless they are altered or enhanced through doping with other materials. The processes of doping and modification come with their own set of technical challenges. Consequently, exploring new methods to develop materials that do not require doping or modification is crucial for achieving a robust and cost-effective sensor technology. Also, the type of fabrication procedure being used affects the overall cost of the device. Exploring simpler fabrication methods is of utmost necessity. ZnO has been the material of choice in this project. Gas sensors that utilize metal oxides are frequently discussed in research, but they often suffer from inadequate selectivity. To improve both selectivity and sensitivity, modifications are necessary, involving the incorporation of various metals such as Pd, Pt, Au, Cu, Ag, etc [14].

Some of the ZnO based gas sensors are mentioned in table 1. The various parameters that are used to compare between sensors are operating temperature, sensor response, recovery time and response time.

The operating temperature is decided as that temperature at which maximum sensor response is obtained. Sensor response is the change in the value of resistance of the sensor when in air versus in the presence of the target gas.

Sr.No	Sensing material	Gas	Operating Temp (°C)	Response (%)	Reference
1.	ZnO flakes	Ethylene	200 °C	17.2	[15]
2.	ZnO nanoparticles	CO	250	74	[16]
3.	ZnO nanowires	NH_3	RT	20	[17]
4.	Au loaded ZnO	NH_3	240	64.5	[18]
5.	Au/ZnO microspheres	CH_4	250	4.16	[19]
6.	ZnO-Ag	Ethylene	RT	19.6	[20]
7.	Ce-doped ZnO	Ethanol	300	72	[21]

Table 1: Some reported ZnO based gas sensors and their parameters

ZnO nanostructures have been synthesized by various procedures[14] from simple methods like hydrothermal to complex methods of film growth like chemical vapor deposition and atomic layer deposition. Use of commercial ZnO has not been satisfactory till date. Our motivation was to explore the use of commercially available ZnO powder to deposit films of high quality and comparable performance to those of the already reported ones. Surprisingly, the film deposition method we used has given excellent results such as high sensor response and fast response and recovery times (<100 s). Also, we have been successfully able to sense the fruit volatiles as demonstrated by our real-time sensing experiments mentioned in Chapter 4.

Numbers fall short of describing the enormous amount of data being generated globally daily. The von Neumann bottleneck has called for increasing research on biologically inspired devices that mimic the neurological system [22]. The main drawback of this architecture is the time required for analysing big data as it relies on shared space for memory and processing which is a performance bottleneck for overall system speed. Memristors used for neuromorphic computing mimic synaptic activity. Memristors are fundamental circuit elements theorized

by Leon Chua in 1980 [23]. Memristors are devices that can mimic the human brain. Traditionally, they are made of TiO_2 [24] which manifests memory due to the migration of oxygen vacancies. Applying a pre-synaptic pulse voltage to the top electrode and recording the post-synaptic current from the bottom electrode is indicative of the memristive conductance. But the other mechanisms based on which memristors can work are the formation and annihilation of conductive channels or by the displacement of ionic species[25,26] . Lithium-ion intercalation materials have a high diffusion coefficient and can adjust Li content in the switching layer . The symmetry and switching speed of the memristor need further improvement for integration into hardware. Li-intercalation materials and battery electrode materials can prove to be good substitutes [6].

Taking inspiration from battery structure, our device structure is as mentioned in Fig.8.

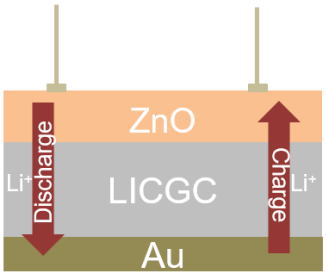

Figure 8: Proposed device structure

Chapter 3: Experimental Section

Materials used:

Zinc oxide ZnO powder was purchased from Sigma Aldrich (99% purity). PVP (polyvinyl pyrrolidone) of molecular weight ~55,000 from Sigma Aldrich was used. NMP (1-Methyl-2-pyrrolidone) of 99.5% purity was procured from Emplura. The trial substrates used were silica and alumina. The final device was fabricated using LICGC having composition Li_2O-Al_2O_3-SiO_2-P_2O_5-TiO_2-GeO_2 (purchased from Ohara corporation). The LICGC is a glass ceramic having high ionic conductivity of up to 10^{-4} S cm at room temperature (comparable to liquid electrolytes [27]. It also has a very low surface roughness which allows for the formation of good contact with the film. Annealing was carried out in a tube furnace.

3.1: ZnO target for sputtering

ZnO targets were prepared by mixing a few drops of 2% PVA solution as a binder with 15g of ZnO powder and then pelletizing it using an SS die and hydraulic press. 2-ton pressure was applied for 5 mins to obtain the pellet and then sintering was done at 900 ^{o}C for 3h to improve the density.

3.2: ZnO film on silica

SiO_2 substrates were polished using a semi-automatic polishing machine, polishing paper of varied grit sizes and polishing liquid (Diamond Suspension 3μ and 1μ). The detailed process is illustrated in Fig.1 (a) and (b). ZnO powder (Sigma Aldrich <5μm particle) was used to make a slurry using PVP (polyvinyl pyrrolidone) in 9:1 ratio with NMP as the solvent. The slurry was ground until a paint-like consistency was obtained. This was drop-casted onto a polished silica surface and spread using a glass slide to obtain a homogeneous, uniform film of ZnO (as shown in Fig. 2). Then it was annealed in a tube furnace at 600 °C

for 2 hours so that the polymer could be decomposed and also for the ZnO film to have a better bond with the substrate. After annealing, 2 ohmic contacts were made on the film using Pt wire and conductive silver paste in order to study the gas sensing behaviour. The prepared thin film was characterized by SEM and AFM to investigate the connectivity between crystallites and their topography.

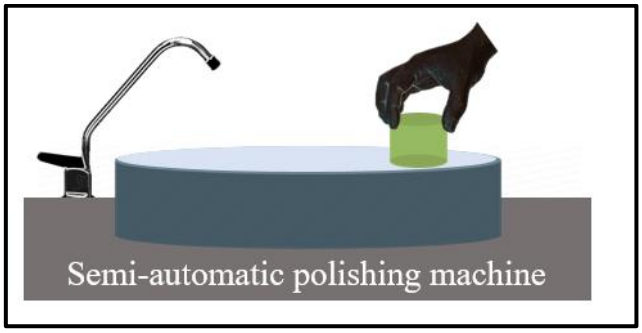

Figure 9: Polishing procedure: The substrate was polished using polishing papers of various grit size and diamond polishing liquids of 3µ and 1µ.

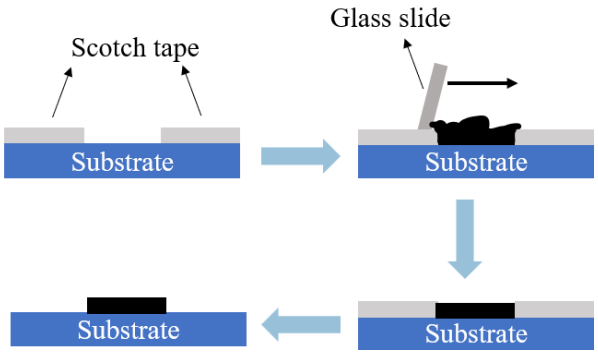

Figure 10: Schematic for doctor blading process

3.3: ZnO film on alumina

Polycrystalline alumina substrate was cut into the required dimensions using a slow speed saw and then polished using semi-automatic polishing machine following the same procedure as in Fig.1(a) and 1(b). ZnO pellet was prepared by pressing commercial ZnO powder mixed with PVA binder in an SS pellet die and then sintering it at 600 °C. The

sintered pellet was used as a target for RF sputtering. The instrumental setup of RF sputtering is shown in Fig.11 .The sputtering was done at room temperature with a substrate-target distance of 7 cm in Ar for 20 mins. Then it was annealed at 600 °C for 2h [28]. Ohmic contacts were made on this using Pt wire and conductive silver paste for further gas sensing studies. The prepared thin film was characterized by SEM and AFM to investigate the connectivity between crystallites and their topography[29].

RF (Radio Frequency) sputtering deposition is a technique used in thin film deposition

1. Setup: In RF sputtering, a target material is placed in a vacuum chamber along with the substrate. The chamber is then filled with an inert gas such as argon using the MFC (mass flow controller).

2. Ionization: An RF power source is applied to create a plasma within the chamber. This plasma ionizes the inert gas atoms, turning them into positively charged ions.

3. Sputtering: The positively charged ions are attracted to the negatively charged target material (the cathode). When these ions collide with the target surface, they transfer their kinetic energy to the target atoms, causing them to be ejected from the target surface. This process is called sputtering.

4. Deposition: The sputtered atoms travel through the vacuum chamber and deposit onto the substrate (the anode), forming a thin film layer. By controlling parameters such as the RF power, gas pressure, and target material composition, the thickness and properties of the deposited thin film can be precisely controlled.

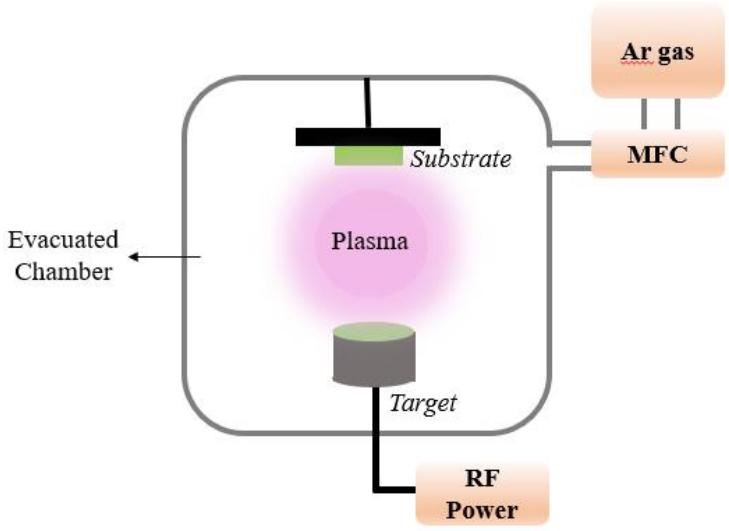

Figure 11: RF Sputtering schematic

Fig.11 shows the experimental setup for RF Sputtering. Thin film deposition techniques are broadly classified as chemical and physical deposition[30]. RF Sputtering does not involve the occurrence of a reaction within the chamber and is hence a type of physical deposition technique.

3.4. ZnO films on LICGC

After the deposition of films on the trial substrates and analysing their properties, the same two methods were employed to deposit ZnO film on the final substrate LICGC. The doctor-bladed and RF-sputtered films were deposited on 2 different LICGC substrates with Au deposited as the bottom electrode. The film thickness was measured using a surface profilometer and was nearly 300 nm[31]. After the fabrication of the complete device, an electrochemical study was performed to confirm the occurrence of the redox process at the ZnO/LICGC interface [32]. Also, the electrochemical properties of the substrate were checked independently as well as with Au blocking electrodes on either side [33]. The final device ZnO/LICGC/Au was analysed by SEM, XRD, AFM and Raman spectroscopy and then used for gas sensing study. 3 ohmic contacts were made: 2 on the ZnO surface and one at the bottom

electrode that was used for performing the lithiation of ZnO by applying an external bias. Also, the electrochemical study of the substrate was done by cyclic voltammetry and electrochemical impedance spectroscopy to understand the phenomena occurring in the system[34].

3.5 Gas Sensing studies

Gas sensing measurements were conducted using a custom gas sensing setup as shown in Fig.8 . A temperature controller was utilized to regulate the sensor's operating temperature. Electrical connections were established by using platinum wire and silver paint for charge transport. Subsequently, the sensor was positioned within a 10L glass chamber. The gas sensor studies were studied by injecting gas into the chamber with a syringe. Current was measured using a picoammeter connected to the user interface software for automated data collection.

Gas concentration was pre-determined using the formula :

$$\text{Gas conc. (ppm)} = \frac{\text{Known injected vol of gas(l)}}{\text{Vol of the chamber(l)}} \times 1000$$

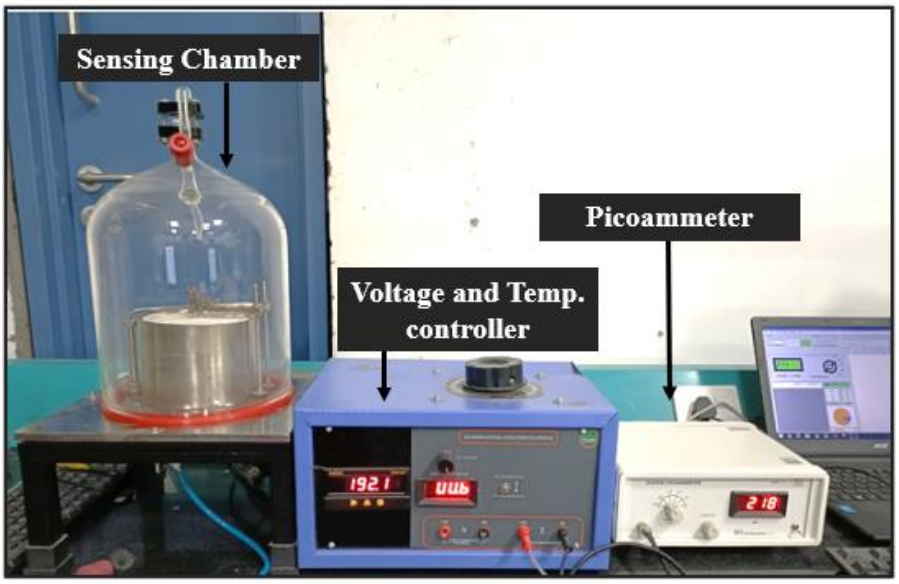

Figure 12: Gas Sensing setup

3.6 Instrumentation

AFM studies were done using Park Systems NX10 Atomic Force Microscopy in non-contact mode (NCM). Supra 55 Zeiss field-emission scanning electron microscope was used to capture the FESEM images. X-Ray Diffraction spectra was analysed by XPert Highscore. Raman studies were carried out using LabRAM HR Evolution Raman Spectrometer. Electrochemical measurements were performed using Metrohm u-1800 potentiostat and Dropview 8400 software.

Chapter 4: Results and Discussion

First, the real-time fruit ethylene production curves have been discussed. Then the characterization of the final device along with the gas sensing properties before and after lithiation have been discussed. A theoretical explanation of the change in electronic properties after insertion of Li into ZnO has been explained briefly. The mechanism of sensing has been discussed based on Oxygen Adsorption model.

For checking the memristive behaviour, I-V characteristics of the device have been performed using a Keithley 2604B Source Measure unit.

4.1 Characterization of ZnO film on silica

The FE-SEM Micrographs and AFM topography images (Fig.13) were recorded for the doctor bladed ZnO sample. There was good connectivity between the crystallites and the film was not very porous. Average roughness of the film was nm which was comparable to that of the films deposited by sputtering.

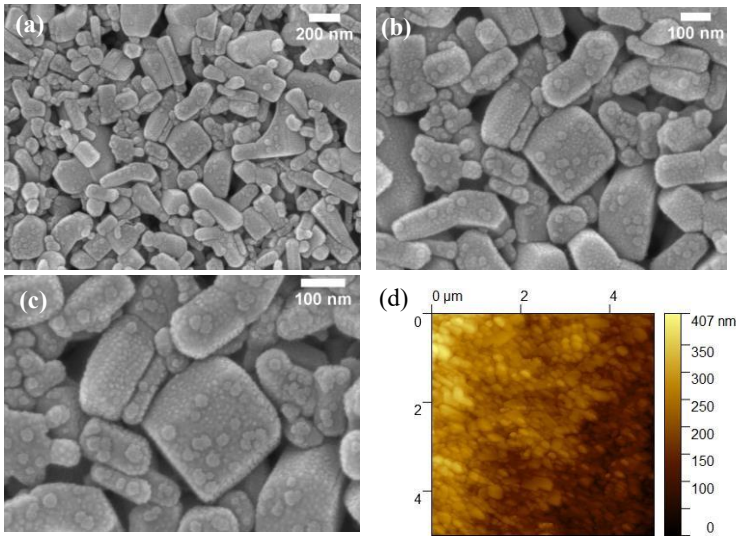

Figure 13: FE-SEM micrographs for the doctor bladed ZnO film on silica substrate at (a)50kx(b) 100kx; (c) 150kx magnification and (d) AFM image for topography of the film

4.2 Ethylene gas and fruit volatiles sensing using ZnO film:

The sensing experiments were carried out by placing the fruit inside the sensing chamber and recording the variation in the current before and after the presence of the fruit. Sensor response was recorded for the fruit to monitor the fruit volatiles production during ripening. Sensor response is calculated by the following formula :

$$SR\ (\%) = \frac{I_{gas} - I_{air}}{I_{air}} \times 100$$

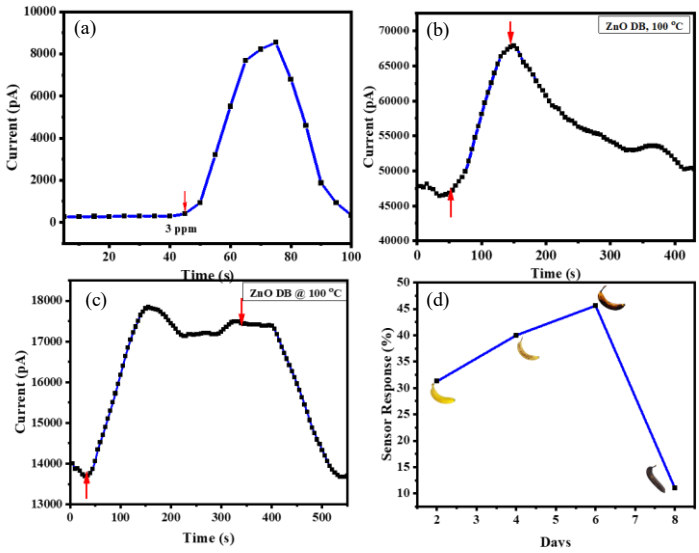

Figure 14: (a) 3 ppm ethylene gas sensing at 100 °C; (b), (c) Real-time response curves of the gas sensor to banana fruit; (d) sensor response at different stages of fruit ripening.

The study indicated that the ZnO film deposited onto silica using a doctor-blade technique can detect the gases released by fruits, and this detection changes over time as the fruits ripen. Figure 14 (a) illustrates the response to 3 ppm of ethylene. Figures 14 (b)-(d) depict the response to fruit gases, measured by enclosing the fruit in the sensing chamber, over several days. The sensor's reaction varied throughout different stages of fruit ripening. Ethylene was identified as the primary component of the fruit gases. Following successful sensing results, the procedure was replicated using LICGC as the substrate for the final device.

4.3 Electrochemical study of LICGC

The substrate used; LICGC; is a complex mixed metal oxide with NASICON structure to facilitate the conduction of Li^+. It has a composition of Li_2O-Al_2O_3-SiO_2-P_2O_5-TiO_2-GeO_2. It has a wide electrochemical window of -3V to 3V. Cyclic voltammograms of the bare LICGC substrate with Pt wire contacts on either side were recorded.

A clear peak is observed at 0.53V and -0.5V which could be attributed to the reduction and oxidation of Ti in Li_xTiO_2 [34]. Further, 10nm of Au was deposited on either side of the LICGC and Pt wire was attached to it to record the cyclic voltammogram. The peaks corresponding to Li-Au alloy formation was observed . It is a multistep alloy formation process. The process of Li-Au alloy formation is briefly mentioned. The requirements for the proper alloy formation include good compatibility between electrodes[5,35].

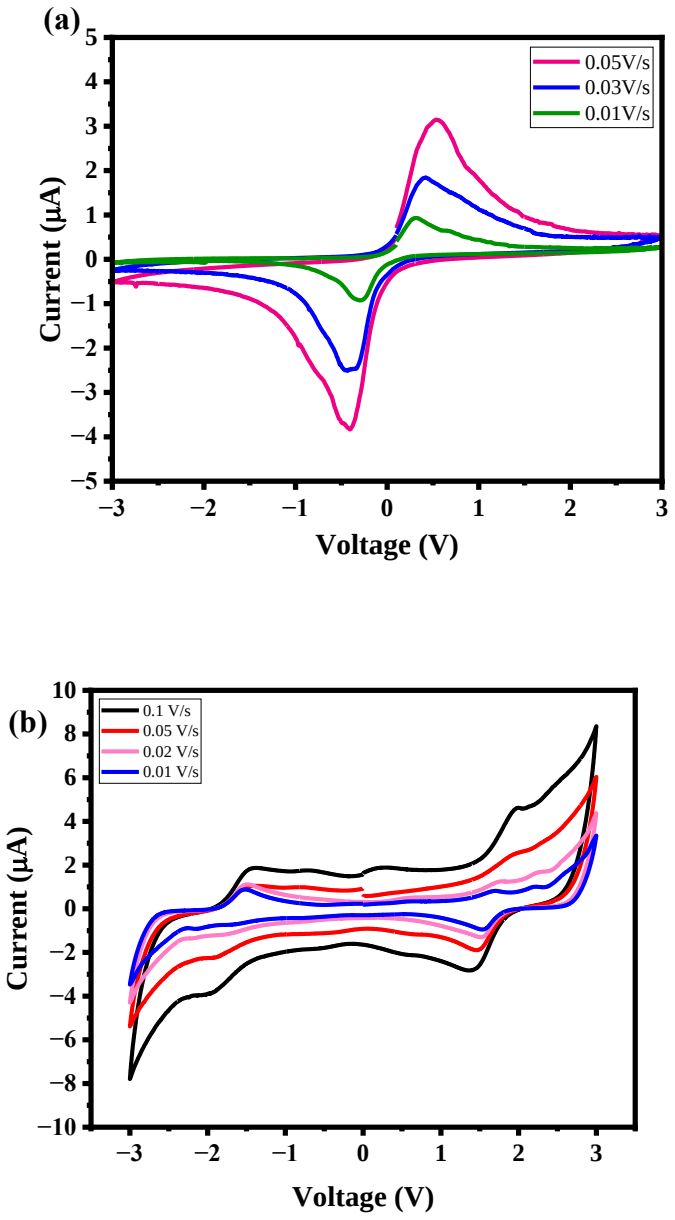

Figure 15: Cyclic voltammograms of (a) bare LICGC with Pt wire contacts and (b) LICGC with 10nm Au electrodes deposited on either side

EIS measurements were performed to compute the Nyquist plot for LICGC with Au blocking electrodes as shown in Fig.16. The semi-circle in the high frequency region was observed due to the interfacial resistance between Au and LICGC. The linearity observed in the low frequency is attributed to the diffusion of Li^+. Diffusion-limited processes are evident at lower frequencies. EIS measurements are conducted over a wide range of frequencies to account for all the processes each of which has a different time scale[36]. The equivalent circuit for a semicircle on the Nyquist plot is a resistor and capacitor in parallel.

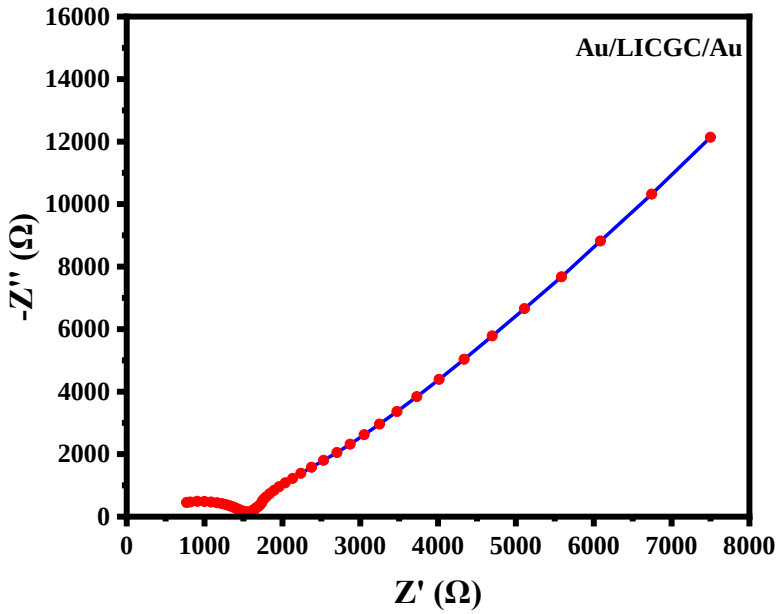

Figure 16 : Nyquist plot for Au/LICGC/Au

For the cyclic voltammogram of the final device, ZnO was kept as the working electrode and voltage was swept from -3V to 0V. A clear redox peak obtained at -0.8 V at higher scan rates of 0.05 V/s and 0.1 V/s in Fig.17 indicates the lithiation of ZnO [37]. This constant potential difference was then applied externally across the 2 electrodes for lithiation and further gas sensing characteristics study. But in the case of

RF Sputtered ZnO device, no redox peaks were observed in the cyclic voltammogram. Thus the lithiation of ZnO was observed only in the doctor bladed film. The quality of the film as assessed by AFM and XRD suggests that the roughness values are nearly identical but the orientation of ZnO crystallites on the substrate varied depending on the method employed for making the film. The gas sensing study was performed only for the doctor bladed film.

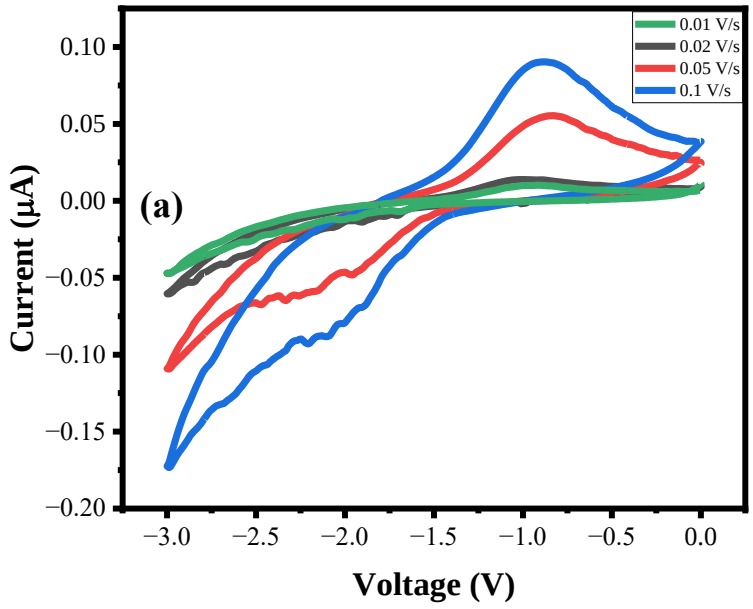

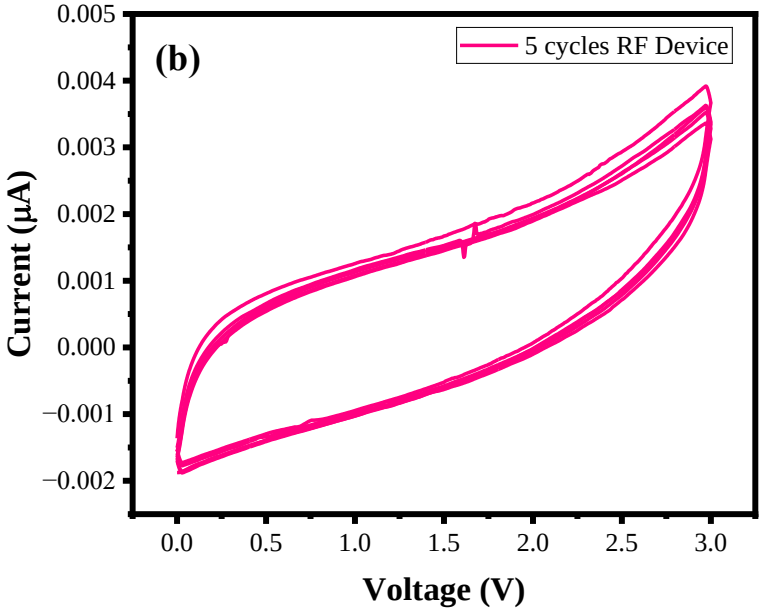

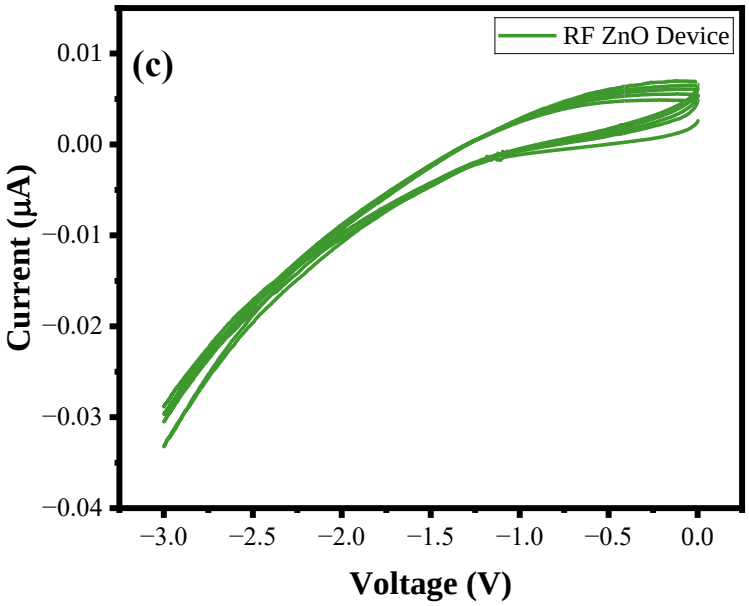

Figure 17: Cyclic voltammogram of the final device ZnO/LICGC/Au (a) by doctor blade method ; (b) and (c) by RF Sputtering

The film deposited on LICGC was also characterized by FE-SEM, AFM, XRD and Raman Spectroscopy. Later, Pt wire contacts were made to study the gas-sensing properties of ZnO film on LICGC.

4.4 Characterization of ZnO film on LICGC

The morphology and composition of the film after annealing was investigated by FE-SEM and EDX analysis. The roughness of the film was 54.9 nm; comparable to one obtained by sputtering. The film thickness was ~ 60 microns. Raman Spectroscopy was used to confirm the lithiation after gas sensing experiments were completed in the pristine state.

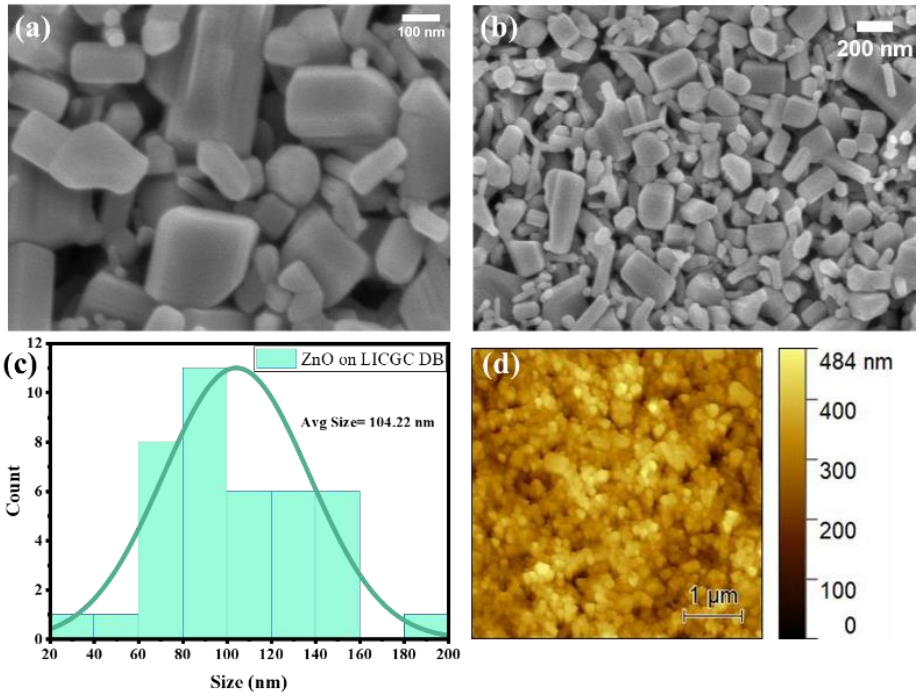

Figure 18: (a),(b)SEM images of the doctor bladed ZnO film on LICGC, (c) Average particle size distribution histogram, (d) AFM images of the film taken in a 5x5 micron area

Elemental mapping was done to confirm the homogeneous distribution across the surface (Fig.19). Also, EDX data confirms the presence of ZnO in the stoichiometric ~1:1 ratio.

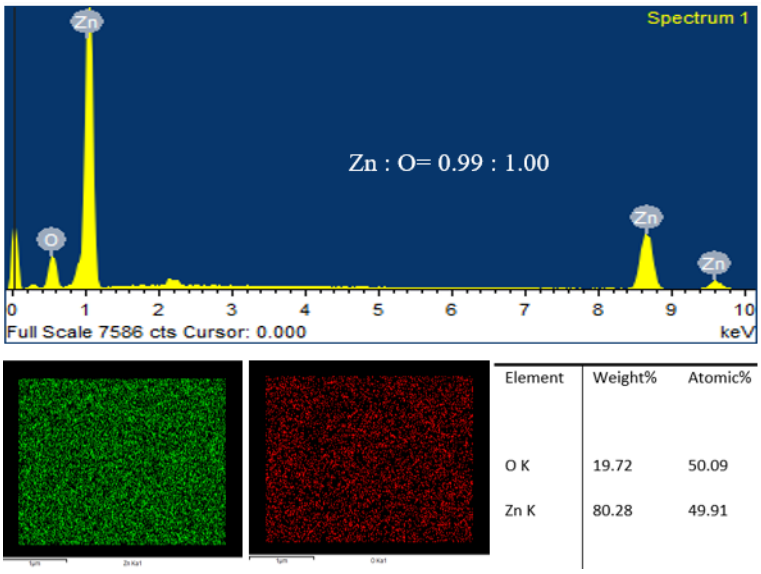

Figure 19: EDX elemental analysis and elemental mapping of the ZnO films. The Zn:O ratio is maintained even after annealing in which indicates that there was no defect formation due to annealing

The similar characterization for RF sputtered films on LICGC was done using FE-SEM and AFM.

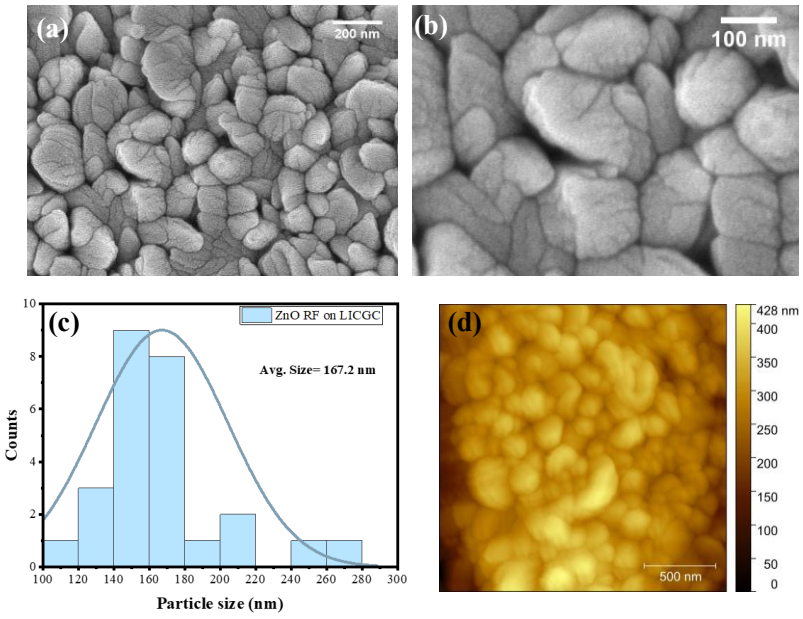

Figure 20: (a) and(b):FE-SEM images of the sputtered film; (c) average particle size distribution from SEM; (d) AFM topography image on a 5x5 micron area

4.5 Ethylene gas sensing study of the device

4.5.1 In the pristine state

The device was connected to the gas sensor and a constant voltage bias of 0.6 V was applied to note the changes in the value of current upon insertion of gas into the chamber. The gas sensing study was done at different operating temperatures and different concentrations. Fig.21 shows the gas sensing curves recorded at an operating temperature of 250 °C for 20, 30 and 50 ppm of ethylene gas.

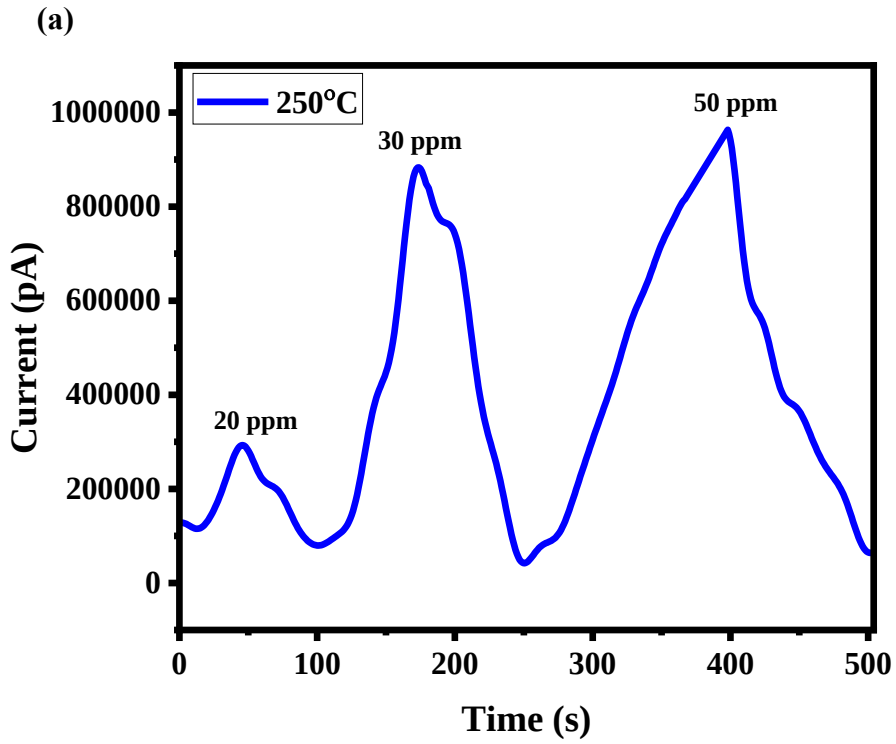

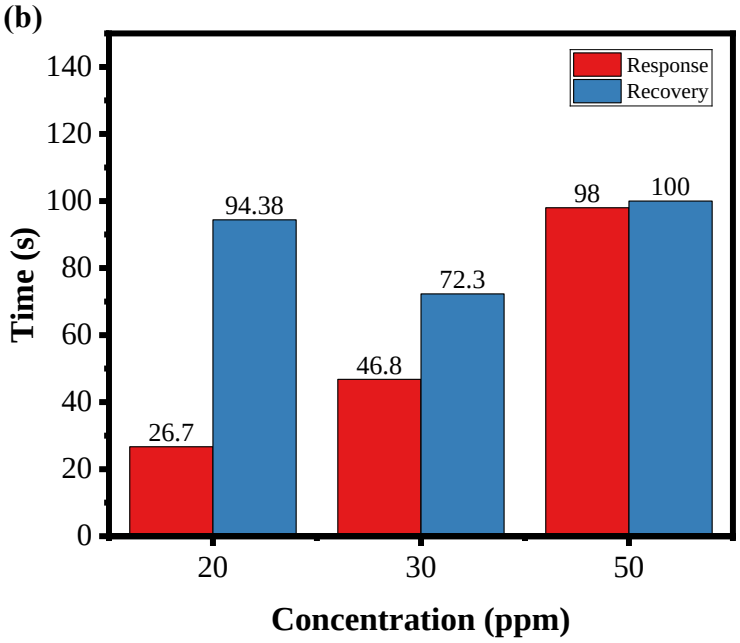

Figure 21: (a) Ethylene gas sensing curves for 20, 30 and 50 ppm of gas at an operating temperature of 250 °C (b) response and recovery times

A very high sensor response of 138.7 %, 675 % and 880 % for 20, 30 and 50 ppm of ethylene respectively was observed. The variation of sensor response to a fixed concentration of gas was measured. It increased linearly with temperature from 50 °C to 250 °C as shown in Fig.22. The sensor responses were 16%, 45%, 60%, 93% and 138.7% respectively.

Such high values of sensor response for ethylene have never been recorded. The film fabrication technique is very facile and yet has a very high sensitivity.

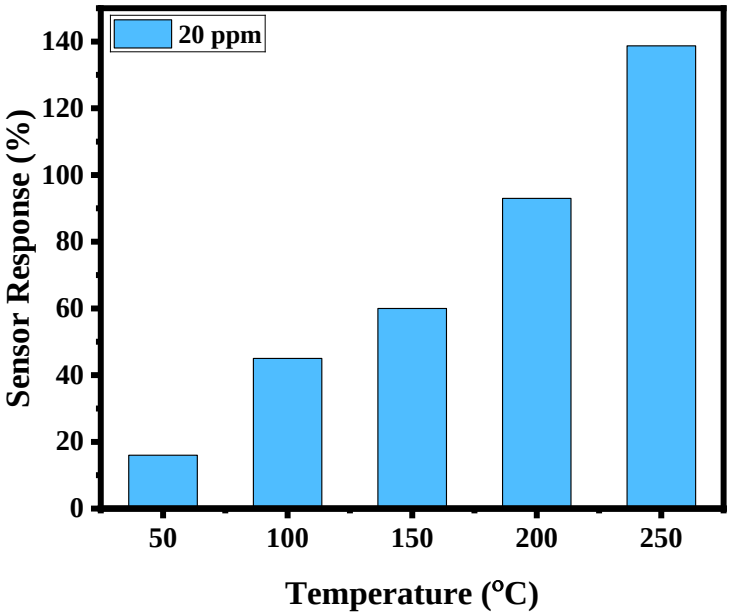

Figure 22: Sensor response for 20 ppm ethylene gas

A good sensor response was also observed at temperatures of 50 °C, 100 °C and 150 °C which is shown below in Fig.23 (a). The corresponding sensing curves for 20 ppm gas have been shown in Fig.23 (b).

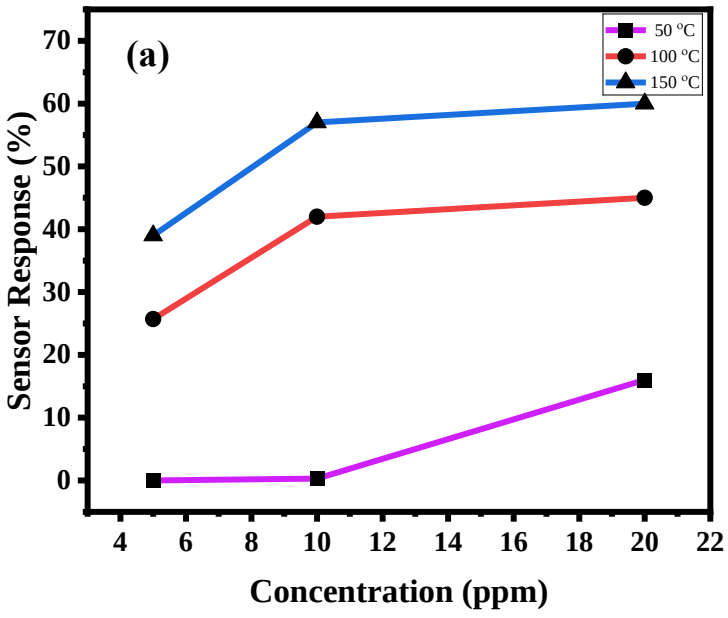

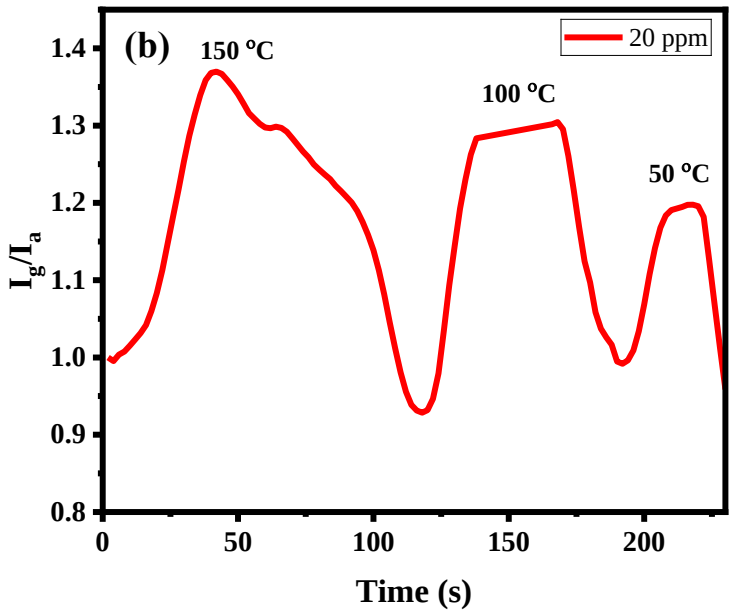

Figure 23: (a) Comparative sensor response to 5, 10 and 20 ppm at 50 °C, 100 °C and 150 °C respectively and (b) Gas sensor response curves at 20ppm concentration

As for the doctor bladed films on silica, we repeated the real-time experiment of ethylene emission from banana at an operating temperature of 100°C. The graph is shown in figure 24. A high sensor response of ~ 60% was achieved.

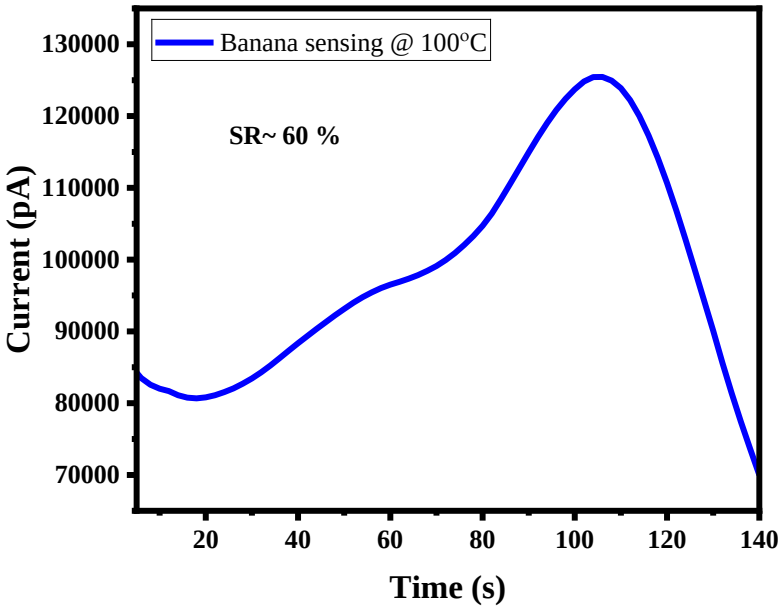

Figure 24: Real time response from fruit at an operating temperature of 100°C

4.5.2 In the lithiated state

All the gas sensing experiments were repeated in the lithiated state to compare the sensor response with pristine state. The comparative sensor response in either state for 20 ppm ethylene gas is shown in Fig. 25. An enhancement in the sensor response is observed upon lithiation. The reason for this has been explained in detail in 4.10. A very high sensor response was observed at 250°C. Such a high response to ethylene gas has never been recorded before. The porous nature of the film due to the decomposition and removal of the PVP binder on annealing has facilitated better adsorption of the gas.

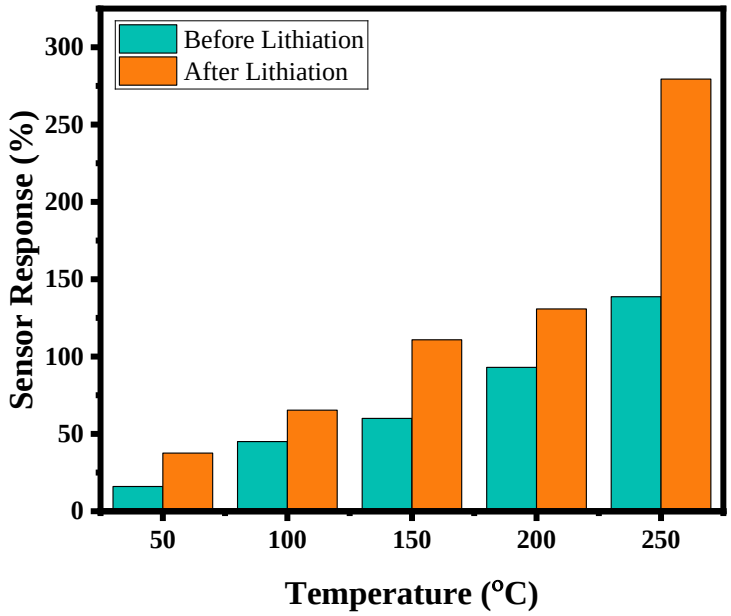

Figure 25: Comparative sensor response to 20ppm of ethylene gas before and after lithiation

The comparative sensor response for 20 ppm gas has also been listed out in Table 2.

Sr. No.	Temperature (°C)	SR(%) before lithiation	SR (%) after lithiation
1.	50	16	37.6
2.	100	45	65.38
3.	150	60	110.8
4.	200	93	130.8
5.	250	138.7	279.4

Table 2: Comparison of sensor response values before and after lithiation

4.6 Confirming of the lithiation of ZnO

Lithiation of ZnO was confirmed with the help of Raman spectroscopy. The Raman spectra were recorded in the pristine and lithiated states. Also, the effect of lithiation of ZnO on the electrical properties was seen in the form of increased resistance which is in accordance with the theoretical data.

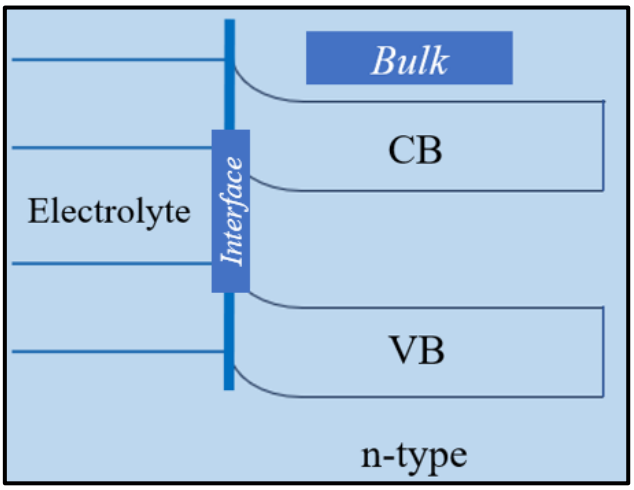

Figure 26: Energy diagram at the solid electrolyte-semiconductor interface

Insertion of Li into the ZnO lattice has distinct structural and electronic changes. The reason for increased resistivity is the fact that Li acts as acceptor impurities and captures the free electrons which act as charge carriers[3839]. A plausible mechanism for the same is mentioned below:

A constant external bias of -0.8V was applied across the top and bottom electrodes to facilitate the lithiation of ZnO. Then, gas sensor characteristics were studied upon lithiation. To confirm lithiation, Raman spectroscopy was used. The pristine state Raman spectrum of ZnO on LICGC and ZnO doctor bladed on LICGC is shown in Fig.25. The excitation wavelength used was 633 nm and 532 nm respectively. The peaks are broader for RF Sputtered ZnO because of the nanostructured phase. The peak obtained at 442 cm^{-1} known as E2 is the

fingerprint for wurtzite structure [40]. The experimental value for bulk ZnO 436 cm^{-1}. However, a blue shift is observed due to nanostructured ZnO. The blue shift observed in Raman spectra for nanostructured materials is a complex interplay of confinement, surface effects, strain, quantum confinement, and size-dependent phonon modes, all of which influence the vibrational properties of the material at the nanoscale.

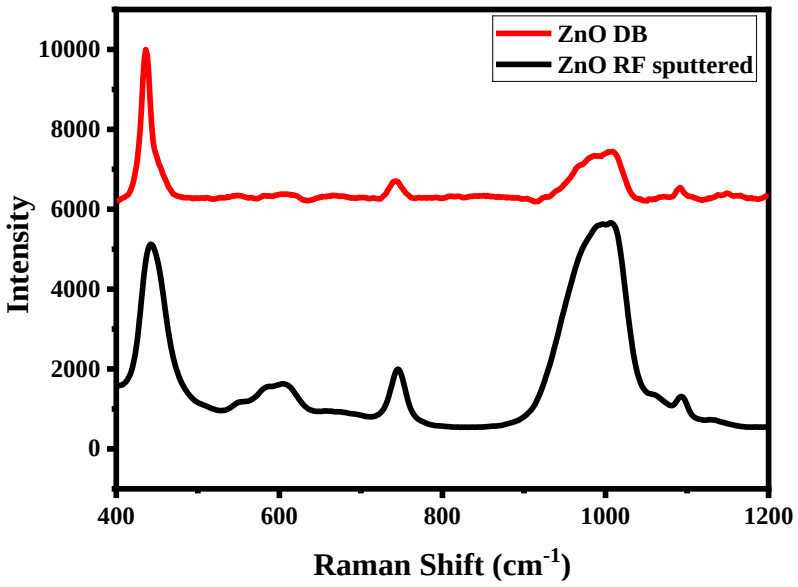

Figure 27: Raman Spectrum of pristine ZnO film sputtered on LICGC

The XRD pattern for RF sputtered ZnO on LICGC is shown in Fig.13. All the diffraction peaks marked in red match with ICSD Number – 00-024-0660 which corresponds to the rhombohedral phase of $LiTi_2(PO_4)_3$ from the LICGC substrate. The indexed peaks match with ICSD Number-01-074-0534 and correspond to the hexagonal wurtzite phase of ZnO with 1 0 0 orientation on the substrate. The crystallite size was measured using the Scherrer equation

$$D = \frac{K\ \lambda}{\beta\ cos\ \theta}$$

and was found to be 20.06 nm. Nanostructures cause the broadening of the peaks.

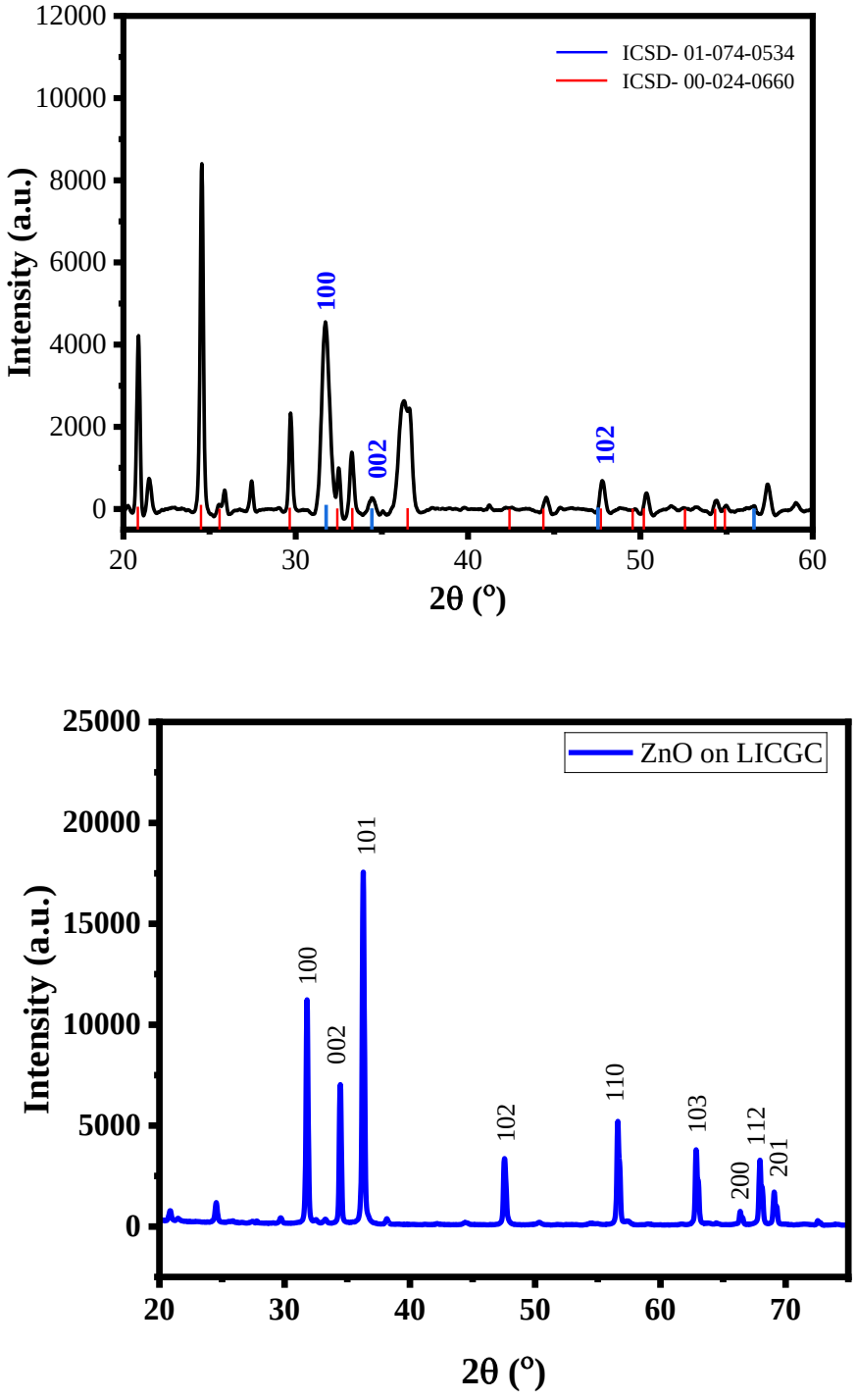

Figure 28:(a) XRD pattern for ZnO deposited on LICGC by RF sputtering[32]; (b) XRD pattern for doctor bladed ZnO film on LICGC

4.7 Selectivity studies

Apart from ethylene, there are other fruit volatiles that occur in comparatively lower amounts. However, the selectivity of the sensor towards ethylene has also been tested against ethanol and acetone. The sensor is selective towards ethylene and can also sense acetone to appreciable levels. Ethanol sensing can be regarded as negligible in comparison to the other 2. Figure 29 shows the sensor response towards the 3 gases at different temperatures.

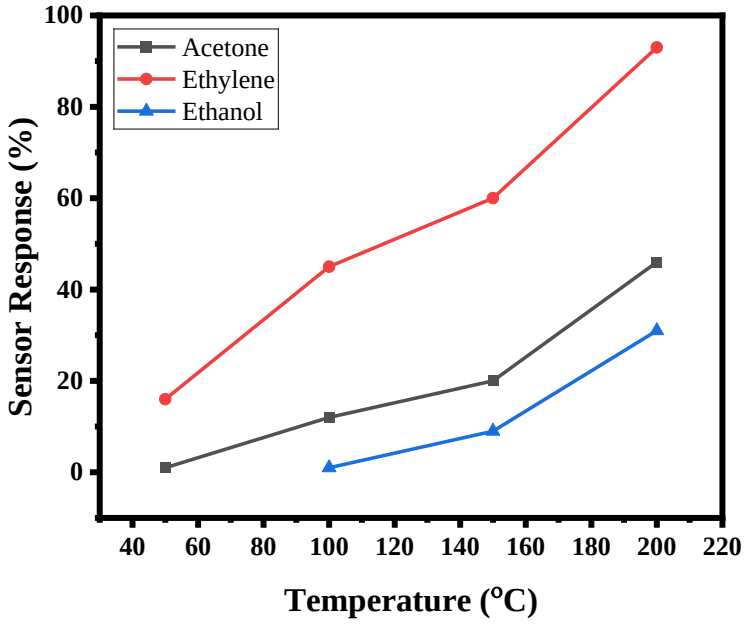

Figure 29: Selectivity of the sensor towards ethylene gas

4.8 Sensing Mechanism

Semiconducting Metal Oxide-based gas sensors are chemoresistive i.e., the resistance varies upon gas adsorption. The most widely accepted mechanism for the variation of resistance is based on the Oxygen adsorption model. In the absence of test gas, there is adsorption of oxygen from the atmosphere. At elevated temperatures, they draw electrons from the conduction band of the metal oxide and form ionized species like O^- and O^{2-}. This causes the depletion region to broaden and hence increases the resistance. When ethylene (reducing gas) is introduced into the chamber, the oxygen adatoms interact with ethylene

and return the electrons into the conduction band of the semiconductor thus reducing the width of the depletion region. This causes the resistance to decrease in the presence of reducing gases. This has been explained schematically in Fig.30. The chemical changes that occur at the interface has been described below.

$$C_2H_4 + O^- \longrightarrow C_2H_4O + e^-$$

$$C_2H_4O + 5\,O^- \longrightarrow 2CO_2 + 2H_2O + 5e^-$$

These electrons are released into the conduction band and reduce the resistance during ethylene adsorption.

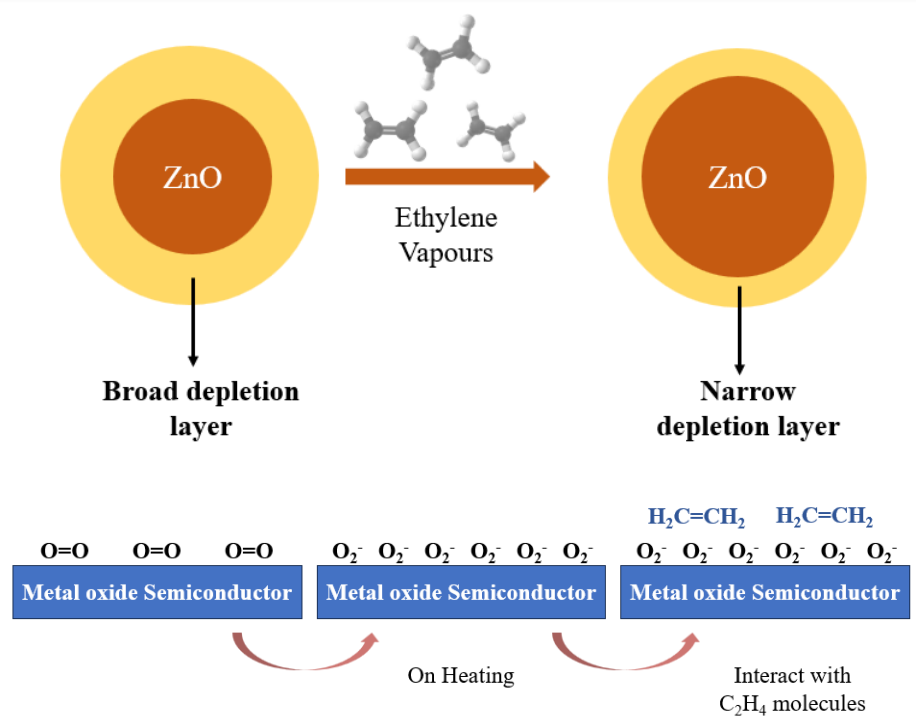

Figure 30: Gas sensing mechanism

4.9 Effect of lithiation on electrical properties of ZnO

When lithium (Li) is added to the zinc oxide (ZnO) lattice, it undergoes unique structural and electrical modifications that profoundly affect its characteristics. Because lithium can easily integrate into the ZnO lattice and has an atomic radius comparable to both zinc and oxygen, it is seen as a great option for doping. This similarity in size ensures that the substitution of zinc by lithium does not cause excessive strain or introduce substantial defects within the crystal structure[41–43].

Lithium can coexist with zinc at interstitial sites (known as Li_{Zn}) or occupy interstitial sites in the ZnO lattice which occurs at lower Li concentrations. The electrical characteristics of ZnO are significantly influenced by the functions of these two distinct lithium locations within the lattice. Li_{Zn} functions as an acceptor impurity. Since free electrons are the main charge carriers in ZnO, these impurities increase the resistivity of the material. This happens because the acceptor impurities capture the free electrons thus increasing the resistance. Li-interstitials, however, act as donor impurities. Under some circumstances, these impurities may even increase the conductivity by donating electrons, so offsetting the electrons that Li_{Zn} acceptors have been able to absorb. The fact that lithium can function as both a donor and an acceptor makes it more difficult to comprehend and forecast the precise consequences of lithium doping in zinc oxide. It implies that to tune the material's qualities for particular applications, a careful balance between different types of impurities is required.

The complexity of Li doping in ZnO highlights the challenges in characterizing and predicting its impact[42]. Extensive research and advanced characterization techniques are required to unravel the intricate balance of these mechanisms.

4.10 Reason for increased sensor response on Lithiation

The introduction of Li into the ZnO lattice creates more oxygen vacancies as Li replaces Zn. These sites are more favourable for oxygen adsorption from the atmosphere. This increase in the adsorption sites facilitates the adsorption of atmospheric oxygen as O_2^- and O^-.Incorporating lithium into ZnO enriches the oxygen concentration on the surface[44]. As the ethylene gas is introduced into the chamber and comes in contact with the ZnO surface, the gas molecules react with the adsorbed ionic oxygen species. Thus, the greater number of reactive sites causes the sensor response to improve significantly.

4.11 Memristor

The I-V characteristics of the same devices were recorded to investigate potential memristive behaviour which can exist due to 2 resistive states: the high resistive state upon lithiation and low resistive state upon delithiation. The following graph shows the I-V Characteristics for the device when a voltage sweep was carried out from 3V to -3V across the top and bottom electrode. The change in the current flowing in the ZnO film was recorded. Further study of I-V characteristics will be needed to reveal the resistive switching mechanisms.

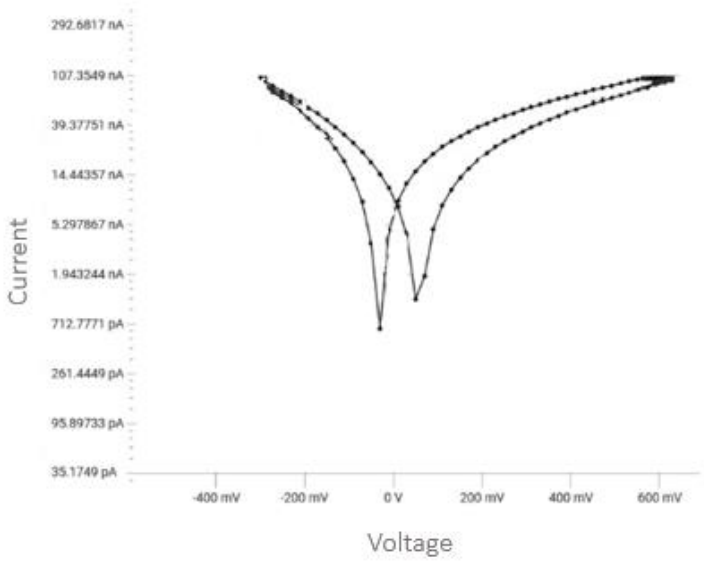

Figure 31: I-V Characteristics of the device with current in semi-logarithmic scale

Chapter 5: Conclusion

In this thesis, we have successfully fabricated a device that can selectively sense ethylene gas that can be useful in agricultural industry. We first used the doctor blade technique to make the film that is widely used in the battery technology but has not been used in gas sensors previously. The porosity and chunk-like morphology was obtained by this method ad annealing after the doctor blading decomposed the binder used leaving behind a porous ZnO film optimum for use in sensing. The film was made on an LICGC substrate which is a Li-ion conducting solid electrolyte and Au was the bottom electrode. The electrochemical study as well as material characterization was performed for the fabricated device using cyclic voltammetry, SEM-EDX, XRD, AFM and Raman Spectroscopy. After this, ethylene gas sensing was checked at various temperatures from 50^{o}C to 250^{o}C. A sensor response of 16% was observed even at temperatures as low as 50^{o}C for 20 ppm of ethylene which explains the high sensitivity of the device . This further increased to 37.6 % upon lithiation of the device by applying external biasing. Chemical methods for doping have been widely explored in literature but this device focuses on a novel strategy of in-situ doping which has been targeted towards gas sensing applications for the first time.

REFERENCES

(1) Terabe, K.; Tsuchiya, T.; Tsuruoka, T. Solid State Ionics for the Development of Artificial Intelligence Components. *Japanese Journal of Applied Physics*. Institute of Physics October 1, **2022**. https://doi.org/10.35848/1347-4065/ac64e5.

(2) T., T. Early History of Solid State Ionics. *MRS Proceedings* **1988**, *135*, 3. https://doi.org/10.1557/PROC-135-3.

(3) Yoshino, A. The Birth of the Lithium-Ion Battery. *Angewandte Chemie - International Edition*. June 11, **2012**, pp 5798–5800. https://doi.org/10.1002/anie.201105006.

(4) Nitta, N.; Yushin, G. High-Capacity Anode Materials for Lithium-Ion Batteries: Choice of Elements and Structures for Active Particles. *Particle and Particle Systems Characterization*. Wiley-VCH Verlag **2014**, pp 317–336. https://doi.org/10.1002/ppsc.201300231.

(5) Palacín, M. R. Recent Advances in Rechargeable Battery Materials: A Chemist's Perspective. *Chem Soc Rev* **2009**, *38* (9), 2565. https://doi.org/10.1039/b820555h.

(6) Zhu, Y.; Gonzalez-Rosillo, J. C.; Balaish, M.; Hood, Z. D.; Kim, K. J.; Rupp, J. L. M. Lithium-Film Ceramics for Solid-State Lithionic Devices. *Nature Reviews Materials*. Nature Research April 1, **2021**, pp 313–331. https://doi.org/10.1038/s41578-020-00261-0.

(7) Yang, S. F.; Hoffman, N. E. Ethylene Biosynthesis and Its Regulation in Higher Plants. *Annu Rev Plant Physiol* **1984**, *35* (1), 155–189. https://doi.org/10.1146/annurev.pp.35.060184.001103.

(8) Sharma, A.; Rout, C. S. Advances in Understanding the Gas Sensing Mechanisms By in Situ and operando spectroscopy. *Journal of Materials Chemistry A*. Royal Society of Chemistry

September 14, **2021**, pp 18175–18207. https://doi.org/10.1039/d1ta05054k.

(9) Caprioli, F.; Quercia, L. Ethylene Detection Methods in Post-Harvest Technology: A Review. *Sens Actuators B Chem* **2014**, *203*, 187–196. https://doi.org/10.1016/j.snb.2014.06.109.

(10) Janotti, A.; Van De Walle, C. G. Fundamentals of Zinc Oxide as a Semiconductor. *Reports on Progress in Physics* **2009**, *72* (12). https://doi.org/10.1088/0034-4885/72/12/126501.

(11) Djurišić, A. B.; Chen, X.; Leung, Y. H.; Man Ching Ng, A. ZnO Nanostructures: Growth, Properties and Applications. *J Mater Chem* **2012**, *22* (14), 6526. https://doi.org/10.1039/c2jm15548f.

(12) Mitra, P.; Chatterjee, A. P.; Maiti, H. S. *Chemical Deposition of ZnO films for Gas Sensors*.

(13) Dey, A.; Roy, S.; Sarkar, S. K. Synthesis, Fabrication and Characterization of ZnO-Based Thin Films Prepared by Sol–Gel Process and H2 Gas Sensing Performance. *J Mater Eng Perform* **2018**, *27* (6), 2701–2707. https://doi.org/10.1007/s11665-018-3284-z.

(14) Kang, Y.; Yu, F.; Zhang, L.; Wang, W.; Chen, L.; Li, Y. Review of ZnO-Based Nanomaterials in Gas Sensors. *Solid State Ion* **2021**, *360*. https://doi.org/10.1016/j.ssi.2020.115544.

(15) Sholehah, A.; Faroz, D. F.; Huda, N.; Utari, L.; Septiani, N. L. W.; Yuliarto, B. Synthesis of ZnO Flakes on Flexible Substrate and Its Application on Ethylene Sensing at Room Temperature. *Chemosensors* **2020**, *8* (1). https://doi.org/10.3390/chemosensors8010002.

(16) Hjiri, M.; Bahanan, F.; Aida, M. S.; El Mir, L.; Neri, G. High Performance CO Gas Sensor Based on ZnO Nanoparticles. *J Inorg Organomet Polym Mater* **2020**, *30* (10), 4063–4071. https://doi.org/10.1007/s10904-020-01553-2.

(17) Selvaraj, B.; Balaguru Rayappan, J. B.; Jayanth Babu, K. Influence of Calcination Temperature on the Growth of Electrospun Multi-Junction ZnO Nanowires: A Room Temperature Ammonia Sensor. *Mater Sci Semicond Process* **2020**, *112*, 105006. https://doi.org/10.1016/j.mssp.2020.105006.

(18) Wang, L.; Lou, Z.; Fei, T.; Zhang, T. Templating Synthesis of ZnO Hollow Nanospheres Loaded with Au Nanoparticles and Their Enhanced Gas Sensing Properties. *J Mater Chem* **2012**, *22* (11), 4767. https://doi.org/10.1039/c2jm15342d.

(19) Zhang, B.; Wang, Y.; Meng, X.; Zhang, Z.; Mu, S. High Response Methane Sensor Based on Au-Modified Hierarchical Porous Nanosheets-Assembled ZnO Microspheres. *Mater Chem Phys* **2020**, *250*, 123027. https://doi.org/10.1016/j.matchemphys.2020.123027.

(20) Sholehah, A.; Karmala, K.; Huda, N.; Utari, L.; Septiani, N. L. W.; Yuliarto, B. Structural Effect of ZnO-Ag Chemoresistive Sensor on Flexible Substrate for Ethylene Gas Detection. *Sens Actuators A Phys* **2021**, *331*, 112934. https://doi.org/10.1016/j.sna.2021.112934.

(21) Zhang, Y.; Liu, Y.; Zhou, L.; Liu, D.; Liu, F.; Liu, F.; Liang, X.; Yan, X.; Gao, Y.; Lu, G. The Role of Ce Doping in Enhancing Sensing Performance of ZnO-Based Gas Sensor by Adjusting the Proportion of Oxygen Species. *Sens Actuators B Chem* **2018**, *273*, 991–998. https://doi.org/10.1016/j.snb.2018.05.167.

(22) Marani, R.; Gelao, G.; Perri, A. G. *A REVIEW ON MEMRISTOR APPLICATIONS*.

(23) Chua, L. 0. *Memristor-The Missing Circuit Element*; **1971**; Vol. 18.

(24) Strukov, D. B.; Snider, G. S.; Stewart, D. R.; Williams, R. S. The Missing Memristor Found. *Nature* **2008**, *453* (7191), 80–83. https://doi.org/10.1038/nature06932.

(25) Ye, C.; Wu, J.; He, G.; Zhang, J.; Deng, T.; He, P.; Wang, H. Physical Mechanism and Performance Factors of Metal Oxide Based Resistive Switching Memory: A Review. *J Mater Sci Technol* **2016**, *32* (1), 1–11. https://doi.org/10.1016/j.jmst.2015.10.018.

(26) Wang, R.; Yang, J.-Q.; Mao, J.-Y.; Wang, Z.-P.; Wu, S.; Zhou, M.; Chen, T.; Zhou, Y.; Han, S.-T. Recent Advances of Volatile Memristors: Devices, Mechanisms, and Applications. *Advanced Intelligent Systems* **2020**, *2* (9). https://doi.org/10.1002/aisy.202000055.

(27) Das, A.; Sahu, S.; Mohapatra, M.; Verma, S.; Bhattacharyya, A. J.; Basu, S. Lithium-Ion Conductive Glass-Ceramic Electrolytes Enable Safe and Practical Li Batteries. *Mater Today Energy* **2022**, *29*, 101118. https://doi.org/10.1016/j.mtener.2022.101118.

(28) Vyas, S.; Giri, P.; Singh, S.; Chakrabarti, P. Comparative Study of As-Deposited ZnO Thin Films by Thermal Evaporation, Pulsed Laser Deposition and RF Sputtering Methods for Electronic and Optoelectronic Applications. *J Electron Mater* **2015**, *44* (10), 3401–3407. https://doi.org/10.1007/s11664-015-3861-y.

(29) Ismail, A.; Abdullah, M. J. The Structural and Optical Properties of ZnO Thin Films Prepared at Different RF Sputtering Power. *J King Saud Univ Sci* **2013**, *25* (3), 209–215. https://doi.org/10.1016/j.jksus.2012.12.004.

(30) Messier, R. Thin Film Deposition Processes. *MRS Bull* **1988**, *13* (11), 18–21. https://doi.org/10.1557/S0883769400063879.

(31) Sharma, S.; Vyas, S.; Periasamy, C.; Chakrabarti, P. Structural and Optical Characterization of ZnO Thin Films for Optoelectronic Device Applications by RF Sputtering Technique. *Superlattices Microstruct* **2014**, *75*, 378–389. https://doi.org/10.1016/j.spmi.2014.07.032.

(32) Tsuchiya, T.; Itoh, Y.; Yamaoka, Y.; Ueda, S.; Kaneko, Y.; Hirasawa, T.; Suzuki, M. A.; Terabe, K. In Situ Hard X-Ray Photoelectron Spectroscopy of Space Charge Layer in a ZnO-Based All-Solid-State Electric Double-Layer Transistor. *Journal of Physical Chemistry C* **2019**, *123* (16), 10487–10493. https://doi.org/10.1021/acs.jpcc.9b01885.

(33) Katzenmeier, L.; Carstensen, L.; Bandarenka, A. S. Li+Conductivity of Space Charge Layers Formed at Electrified Interfaces between a Model Solid-State Electrolyte and Blocking Au-Electrodes. *ACS Appl Mater Interfaces* **2022**, *14* (13), 15811–15817. https://doi.org/10.1021/acsami.2c00650.

(34) Cao, C.; Melegari, M.; Philippi, M.; Domaretskiy, D.; Ubrig, N.; Gutiérrez-Lezama, I.; Morpurgo, A. F. Full Control of Solid-State Electrolytes for Electrostatic Gating. *Advanced Materials* **2023**, *35* (18). https://doi.org/10.1002/adma.202211993.

(35) He, D.; Cui, W.; Liao, X.; Xie, X.; Mao, M.; Sang, X.; Zhai, P.; Zhao, Y.; Huang, Y.; Zhao, W. Electronic Localization Derived Excellent Stability of Li Metal Anode with Ultrathin Alloy. *Advanced Science* **2022**, *9* (10). https://doi.org/10.1002/advs.202105656.

(36) Lazanas, A. C.; Prodromidis, M. I. Electrochemical Impedance Spectroscopy─A Tutorial. *ACS Measurement Science Au*. American Chemical Society June 21, **2023**, pp 162–193. https://doi.org/10.1021/acsmeasuresciau.2c00070.

(37) Ma, X.; Luo, W.; Yan, M.; He, L.; Mai, L. In Situ Characterization of Electrochemical Processes in One Dimensional Nanomaterials for Energy Storages Devices. *Nano Energy* **2016**, *24*, 165–188. https://doi.org/10.1016/j.nanoen.2016.03.023.

(38) Srivastava, J. K.; Agarwal, L.; Bhattacharyya, A. B. Electrical Characteristics of Lithium-Doped ZnO Films. *J Electrochem Soc* **1989**, *136* (11), 3414–3417. https://doi.org/10.1149/1.2096463.

(39) Zhou, Z.; Kato, K.; Komaki, T.; Yoshino, M.; Yukawa, H.; Morinaga, M.; Morita, K. Effects of Dopants and Hydrogen on the Electrical Conductivity of ZnO. *J Eur Ceram Soc* **2004**, *24* (1), 139–146. https://doi.org/10.1016/S0955-2219(03)00336-4.

(40) Kadari, A. sadek; Ech-Chergui, A. N.; Mukherjee, S. K.; Velasco, L.; Singh, R. K.; Mohamedi, M. walid; Akyildiz, E.; Zoukel, A.; Driss-Khodja, K.; Amrani, B.; Reda Chellali, M. Atomic Mapping of Li:ZnO Thin Films and Its Spectroscopic Analysis. *Inorg Chem Commun* **2021**, *132*. https://doi.org/10.1016/j.inoche.2021.108852.

(41) Aksoy, S.; Polat, O.; Gorgun, K.; Caglar, Y.; Caglar, M. Li Doped ZnO Based DSSC: Characterization and Preparation of Nanopowders and Electrical Performance of Its DSSC. *Physica E Low Dimens Syst Nanostruct* **2020**, *121*, 114127. https://doi.org/10.1016/j.physe.2020.114127.

(42) Lu, J. G.; Zhang, Y. Z.; Ye, Z. Z.; Zeng, Y. J.; He, H. P.; Zhu, L. P.; Huang, J. Y.; Wang, L.; Yuan, J.; Zhao, B. H.; Li, X. H. Control of P- and n-Type Conductivities in Li-Doped ZnO Thin Films. *Appl Phys Lett* **2006**, *89* (11). https://doi.org/10.1063/1.2354034.

(43) Hjiri, M.; Aida, M. S.; Lemine, O. M.; El Mir, L. Study of Defects in Li-Doped ZnO Thin Films. *Mater Sci Semicond Process* **2019**, *89*, 149–153. https://doi.org/10.1016/j.mssp.2018.09.010.

(44) Kim, M. Y.; Lee, S. Y.; Kim, J.; Park, C. O.; Shi, W.; Min, H.; Kim, S.; Kim, H.-S.; Shim, Y.-S.; Lee, B. Z.; Choi, M. S.; Jeong, H. M.; Chun, D. W.; Lee, K. H. Generation of Nanogaps on Porous ZnO Sheets via Li-Ion Implantation: NO_2 Gas Sensing with Ultrafast Recovery Time. *Sens Actuators B Chem* **2023**, *379*, 133283. https://doi.org/10.1016/j.snb.2022.133283.